Numerical Analysis of Graphene Cladded Optical Fibre

Ferdinand A. Katsriku[1]*, Grace G. Yamoah[1] and J-D Abdulai[1]
[1]Department of Computer Science, University of Ghana
***Corresponding author:** fkatsriku@ug.edu.gh

ABSTRACT

Graphene has been hailed as a material with extraordinary properties capable of transforming many scientific and industrial fields. In this work, the vector H-field finite element method is used in the characterization of a graphene cladded fibre. Results are presented on the modal analysis of various types of graphene cladded optical fibres. Such fibres may find use as nonlinear elements in linear pulse compression schemes for ultra fast pulse generation.

Keywords: Graphene, FEM, vector H-field, waveguide, optical fibre

Introduction

Integrated all-optical devices will be fundamental in future communication systems. As an essential component of communication systems, these optical devices will act as switches, multiplexers, modulators, reflectors, etc. Research has shown that by perfectly reflecting the waves over the frequency range of interest, or confining propagation in a specified direction and controlling the optical properties of the material, high-speed data transmission could be achieved. Photonic crystal (PhC) technology has made it possible to manipulate light in a way that is not feasible with conventional optical technology. The last two decades has seen tremendous advances in the development of femtosecond laser systems. In particular, optical pulses with temporal widths of a few hundredths of a second or at most a few picoseconds are predicted to be central to ultra fast communications systems and will find application in many domains, including biomedical applications such as optical coherence tomography, laser eye surgery, metallurgy, chemistry, optical signal processing, sensing and terahertz (THz) wave generation.

Recently a new material "graphene", which is an allotrope of carbon, has been investigated and proven to be an optoelectronic material with excellent parameters, namely its chemical, magnetic, thermal and electrical properties. Graphene is a single layer 2-D atomic crystal of carbon with a hexagonal honeycomb structure. Studies have found that a graphene-integrated medium is amenable to convenient tuning of its electronic and optical properties by varying the applied voltage. This property is the prime requirement for an optical waveguide material, and it has spurred a spate of activities within the research community to undertake a study of graphene in the optical waveguide domain. It has been suggested that graphene could be used as saturable absorber in femtosecond laser systems (Bonaccorso *et al.*, 2011; Pumera, 2011; Sun *et al.*, 2010; Zhang *et al.*, 2009; Bao *et al.*, 2009). The literature on graphene has grown quite rapidly in recent years, an indication of the level of interest in this new material within the research community. Graphene has been proposed for use in the design of electro-optic modulators, waveguides, transistors and integrated circuits, and recently it has been suggested as a saturable absorber in a femtosecond pulse generation scheme (Bonaccorso *et al.*, 2011) in order to achieve mode locking. The use of graphene as a saturable absorber offers the possibility of building more compact laser systems. In a saturable absorber, the absorption of light will decrease as the intensity of

the laser beam increases. Until recently, mode-locking was achieved by the use of semiconductor saturable absorber mirrors. However, their low damage threshold, limitations on design flexibility and the carrier relaxation time which limits the pulse width have necessitated the search for new systems. The operation of such mode locked lasers is very complicated, as all the parameters associated with its operation are interdependent on each other, so that minor changes in one parameter could lead to major changes in the laser output (Inoue and Namiki, 2008). Another well-established method for obtaining ultra-short pulses is to use a pulse compression within an optical fibre. This method is applicable to any continuous wave laser source and is more stable because it is based on the intrinsic properties of the travelling wave within the fibre. These methods may suffer from large pedestal and require the use of nonlinear elements, usually dispersion shifted fibre of several hundred metres or even kilometres length of fibre.

Liu *et al.* (2011) demonstrated a broadband, high-speed, waveguide-integrated electro-absorption modulator based on monolayer graphene, paving the way for graphene-based nonlinear photonics. It has high electron mobility and optical transparency, in addition to flexibility, robustness and environmental stability (Bonaccorso *et al.*, 2011). It is found that to fully utilize graphene's remarkable optical properties, it needs to be integrated into planar photonic systems (Li *et al.*, 2012). Studies have shown that the behavior of light in graphene could be tuned electrically, and the converse may also be feasible (Keilmann, 2012). Since light is confined to nanocables with dimensions of a millionth of a millimeter, switching times could be reduced to less than picoseconds (Keilmann, 2012). Thus, integrating graphene with an optical waveguide can greatly increase the interaction length through the coupling between evanescent waves and graphene.

Following this possibility, a team of researchers in UC Berkeley built a tiny optical device that uses graphene to switch light on and off in a graphene/silicon hybrid waveguide structure (Liu *et al.*, 2011). This switching ability is the fundamental characteristic of a network modulator, which controls the speed at which data packets are transmitted. The faster the data pulses are sent out, the greater the volume of information that can be sent (Liu *et al.*, 2011). The speed of data transmission depends on how quickly the modulator can pulse light. Further, studies have shown that when the Fermi level of graphene is tuned, the optical absorption of graphene can be altered. Operating at 1.2 GHz without any temperature controller, such a graphene-integrated modulator has a broad bandwidth (from 1.3 to 1.6 μm) and a small footprint (~25 μm^2) (Liu *et al.*, 2011). The research found that a graphene modulator achieved a modulation speed of 1 GHz and could theoretically reach as high as 500 GHz (500 billion cycles a second) (Liu *et al.*, 2011).

A review of current literature shows that research on graphene is mainly focused on experimental evaluation. The ability to predict the performance of a device before its practical fabrication can be a key factor in the development of new and innovative technologies. In this regard, modeling and simulating a device by the use of a numerical method to predict its performance can lead to reduction in time, cost and constraints involved in experimentation as well as performance optimization. Numerical methods have experienced a resurgence expansion in all fields of engineering due to the exponential growth in the computational power currently available. Recently, results from the numerical characterization of a graphene based terahertz device have been reported. (Themistos *et al.*, 2014).

In this present work, we present results on the modal numerical analysis of various types of graphene cladded optical fibres. Such fibres may find use as nonlinear elements in linear pulse compression schemes.

Numerical Formulation

The key ideas in the finite element method are to:

- discretize the domain under investigation into sub-domains or elements. The accuracy of the method depends on the level of discretization. It is recommended that more elements be used in areas where the field is thought to have steep variations. It is also not advisable to use elements across physical boundaries or interfaces. For symmetrical domains, the mesh should follow the same type of symmetry.
- the functionals for which the variational principle should be applied for the elements are then derived. In deciding on the interpolation function, certain continuity conditions must be satisfied by the interpolation function across inter-element boundaries. These requirements are normally obvious from a physical examination of the problem. It is however also necessary that the function is an admissible member of the Ritz and Galerkin methods. It follows that the polynomial function must remain unchanged under a linear transformation from one co-ordinate system to the other.
- assemble all the element contributions to form a global matrix.
- solve the system of equations that is obtained, in this case a matrix equation.

Hence, instead of differential equations for the system under investigation, variational expressions are derived and the piecewise continuous function approximated by a piecewise continuous polynomial within each element. From the equivalent discretized model contribution from each element, an overall system is assembled. This can be regarded as a sub-class of the Ritz-Galerkin method in which the trial functions are replaced with polynomial functions.

Given the following Helmholtz equation

$$\nabla^2\phi + k^2\phi = 0 \qquad 1$$

as the governing equation in a waveguide problem, defined within the domain Ω, where ϕ is the electric or magnetic field component, ∇^2 is a Laplacian operator defined as

$$\nabla^2 = \frac{\partial^2}{\partial x^2} + \frac{\partial^2}{\partial y^2} + \frac{\partial^2}{\partial z^2} \qquad 2$$

and k^2 is a constant related to frequency, and given also that Γ_f and Γ_n are boundaries within the said domain, then the following boundary conditions may be defined:

$\phi = \hat{\phi}$ on the boundary Γ_f (Dirichlet boundary condition) 3

$\frac{\partial\phi}{\partial n} = \boldsymbol{n}\cdot\nabla\phi = \hat{\psi}$ on the boundary Γ_n (Neumann boundary condition) 4

where $\boldsymbol{n}$ is the outward normal unit vector. The gradient operator is defined by the following matrix differential operator

$$\nabla = \begin{bmatrix} \partial/\partial x \\ \partial/\partial y \\ \partial/\partial z \end{bmatrix} \qquad 5$$

in the Cartesian system of co-ordinates. Taking into consideration the stated boundary conditions, the functional for equation (1) could be written as (Koshiba, 1990)

$$F = \frac{1}{2}\iiint_{\Omega}\left[(\nabla\phi)^2 - k^2\phi^2\right]d\Omega - \int_{\Gamma_n}\phi\hat{\psi}\,d\Gamma \qquad 6$$

The stationary requirement of the above functional, $\delta F = 0$, coincides with the governing equation of the problem. The Neumann boundary condition is automatically satisfied in the variational procedure; as such it is referred to as the natural boundary condition. The Dirichlet boundary condition however needs to be imposed, and is therefore called the forced boundary condition. The functional for each of the elements of the region could then be written as

$$F_e = \frac{1}{2}\iiint_{e}\left[(\nabla\phi)^2 - k^2\phi^2\right]d\Omega - \int_{\Gamma_e}\phi\hat{\psi}\,d\Gamma \qquad 7$$

The functional for the whole of the domain can then be regarded as a summation of the element functions

$$F = \sum_e F_e \qquad 8$$

For the n nodes within each element, the field ϕ can be approximated as follows

$$\phi = \sum_{i=1}^{n} N_i \, \phi_i \qquad 9$$

where ϕ_i is the i^{th} nodal parameter of the element e and N_i is the interpolation or shape function. The above equation could be written in matrix form as follows:

$$\phi = \{N\}^T \{\phi\}_e \qquad 10$$

where the component of the vector $\{\phi\}_e$ is ϕ_i and that of the vector $\{N\}^T$ is the interpolation function N_i. T denotes a transpose, $\{\cdot\}$ and $\{\cdot\}^T$ denote a column and row vector respectively.

For convergence of the solution, the shape function N_i must satisfy certain conditions when the functional contains first order derivatives:

- the variable ϕ and its derivatives must include constant terms
- the variable ϕ must be continuous at the interface of two adjacent elements.

The first of the two conditions is also known as the completeness condition and is simple to satisfy provided complete polynomial expressions are used in each element. The second of the two conditions is called the compatibility condition.

For the accurate characterisation of general waveguides, a vector formulation with at least two field components is required. There are two main types of the full vector formulations, namely the **E**-field and **H**-field. The vector **E**-field approach was first applied by English and Young (1971). This formulation is suitable for generally anisotropic and loss-less problems. The natural boundary condition corresponds to a magnetic wall and as such it is essential to enforce the electric wall as the boundary condition (**n**x**E**=0). Such a condition is quite difficult to impose for an irregular structure. It also requires an additional integral to ensure the continuity of the fields at the dielectric interfaces. The **H**-field formulation, on the other hand, has as its natural boundary condition the electric wall, and the magnetic field is continuous everywhere. As such, it is suitable for dielectric waveguide problems, as no boundary conditions need to be imposed. This formulation is given as

$$\omega^2 = \frac{\int (\nabla \times \mathbf{H})^* \cdot \hat{\varepsilon}^{-1} \cdot (\nabla \times \mathbf{H}) d\Omega}{\int \mathbf{H}^* \cdot \mu^{-1} \cdot \mathbf{H} d\Omega} \qquad 11$$

The above formulation leads to non-physical or spurious solutions since the divergence condition $\nabla \cdot \mathbf{H} = 0$ is not satisfied. Various methods exist for detecting these spurious modes. A simple way is to examine the field profiles: since these modes are characterised by inconsistency and a random variation of the field, they are easy to identify. The mathematical idea underpinning the physical solution is that the condition $\nabla \cdot \mathbf{H} = 0$ is obeyed by the eigenvector. By calculating $\nabla \cdot \mathbf{H}$ for each eigenvector, it is possible to identify the true solutions from the spurious ones. The objective, however, is not simply to detect these modes, but to eliminate them or at least suppress them. The penalty-function method (Rahman and Davies, 1984) is one of the best established methods for eliminating these spurious solutions. The method includes an additional term α, the penalty term, a dimensionless number in the variational formulation, which now is written as:

$$\omega^2 = \frac{\int (\nabla \times \mathrm{H})^* \hat{\varepsilon}^{-1}(x,y)(\nabla \times \mathrm{H}) d\Omega + \alpha \int (\nabla \cdot \mathrm{H})^* (\nabla \cdot \mathrm{H}) d\Omega}{\int \mathrm{H}^* \cdot \hat{\mu} \cdot \mathrm{H} d\Omega} \qquad 12$$

In the above α is a dimensionless penalty term used to compensate for the divergence of the H field. ω defines the angular frequency, and the vector magnetic field at the various nodal points is defined through H. Equation (12) may be minimised with respect to the H field in the

various axial directions to yield a stationary solution, as in Katsriku (2000):

$$[A]\{x\} - \omega^2[B]\{x\} = 0 \qquad 13$$

As in [23], $[\square]$ is a Hermitian matrix of the complex type, $[B]$ is a positive definite real symmetric matrix, ω^2 and $\{x\}$ represent the eigenvalue and eigenvector respectively. Equation (13) can be solved using any standard matrix routine to obtain the field values at the nodes. In this work, required routines were developed using Fortran language.

Numerical Results and Discussion

The two configurations of an optical fibre considered are shown diagrammatically in Fig. 1A and Fig. 1B. In one of the configurations, Fig. 1A, the core of the fibre is cladded with graphene as the outer layer. In the second configuration, Fig. 1B, the graphene is sandwiched between an inner fibre core and an outer fibre cladding. In the simulations, the number of layers of the graphene was either one or two.

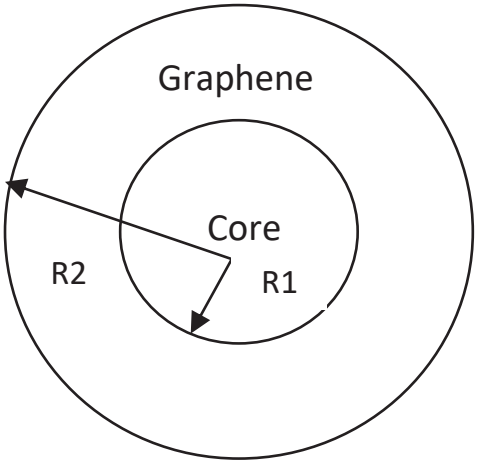

Fig. 1: A) A graphene cladded fibre with no outer cladding

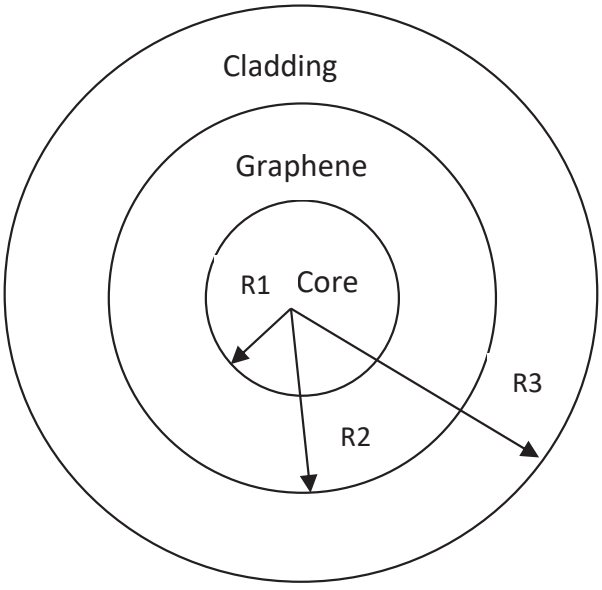

Fig. 1: B) Showing graphene sandwiched between the core and the cladding

In the simulations, the refractive index of the core region was assumed to be 1.49 and the complex refractive index of the graphene region is taken to be 3.51-i14.0 (Themistos *et al.*, 2014). A key issue with numerical simulation involving graphene is its atomic dimension, 3.5 angstrons, which is a thousandth smaller than the other regions. The numerical stability of the solutions was therefore initially tested and the results are depicted in Fig. 2.

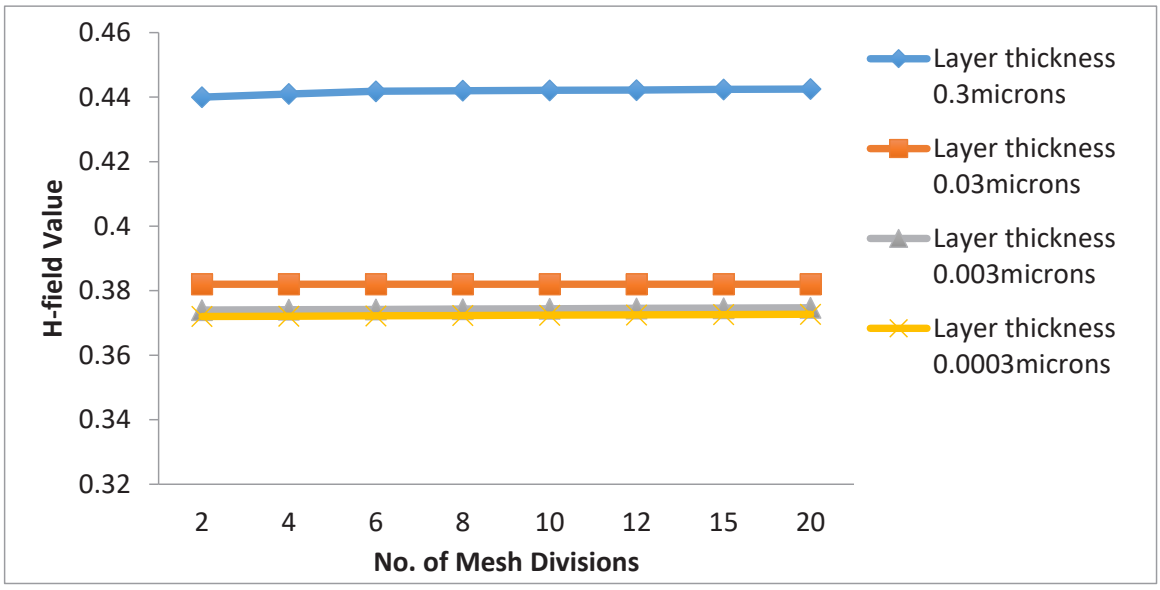

Fig. 2: Showing the stability of the numerical solution as mesh size is varied

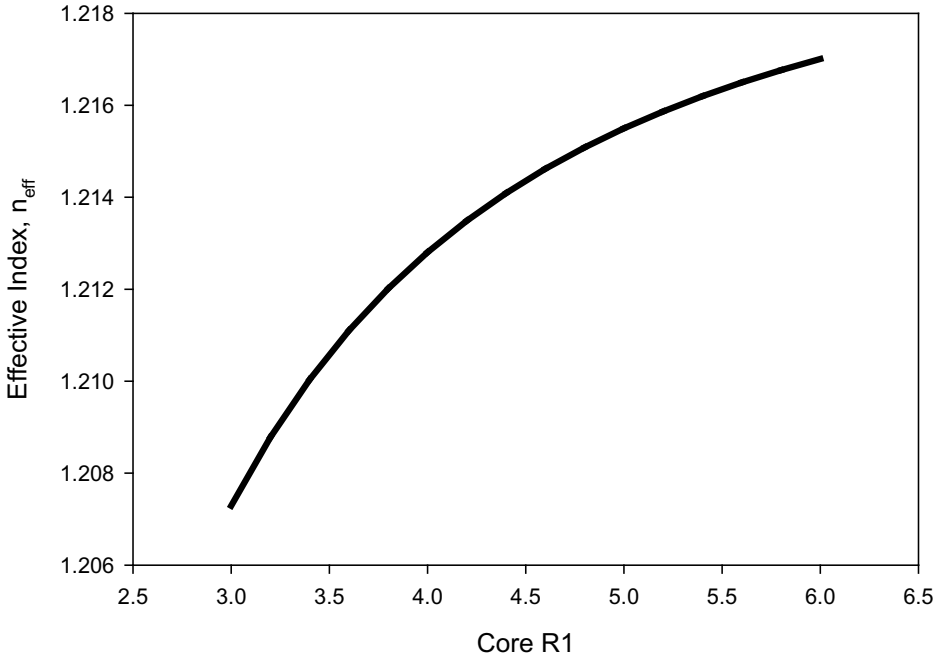

Fig. 3: Showing the dependence of the effective index on the core radius of the fibre

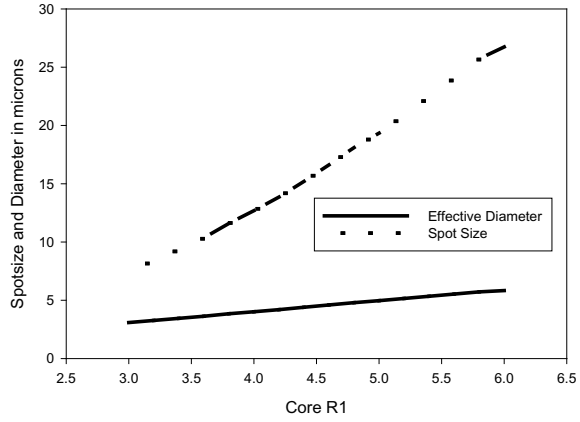

Fig. 4: A) Showing the dependence of the spot size and effective diameter on the width of the fibre core

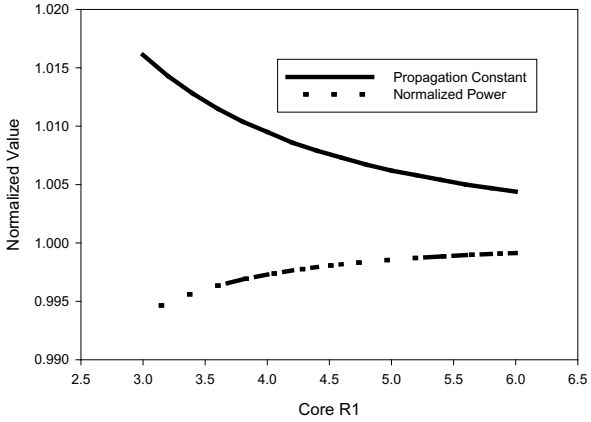

Fig. 4: B) Showing the dependence of the normalized values of power and propagation constant on core size

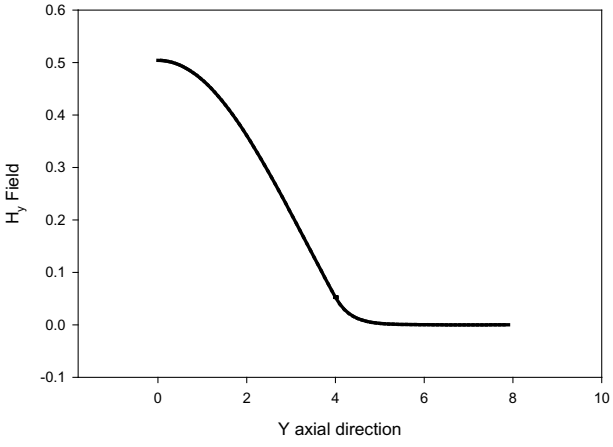

Fig. 5: A) H_y Field profile in the Y-axial direction

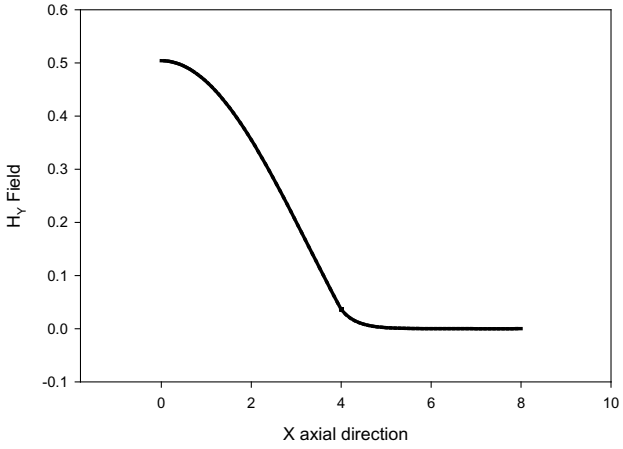

Fig. 5: B) H_y Field profile in the X-axial direction

Hypothetically large widths were chosen equivalent to a thousand layers, hundred layers, ten layers and a single layer of graphene. As can be seen, the results are numerically stable with increasing mesh divisions. In Fig. 3 shows the dependence of the effective index of the fundamental Hy mode of the fibre on the radius of the core dimension. In this, it is assumed that there is no outer cladding, i.e. the configuration of Fig. 1A is used. In Fig. 4A it is seen that as the fibre core is increased, the spot size and the width also increase. Fig. 4B shows the normalized values of power and propagation constant for varying core dimension. It can be seen that when the dimension of the fibre core is increased power also increases whilst the propagation constant decreases.

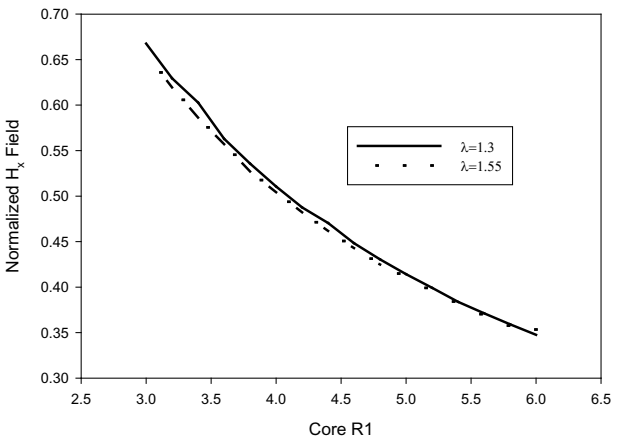

Fig. 6: Showing the normalized field profile as a function of the core radius

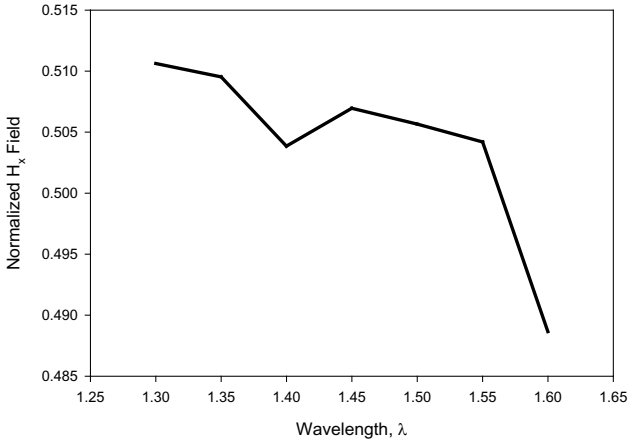

Fig. 7: Normalized H_y Field profile as a function of wavelength

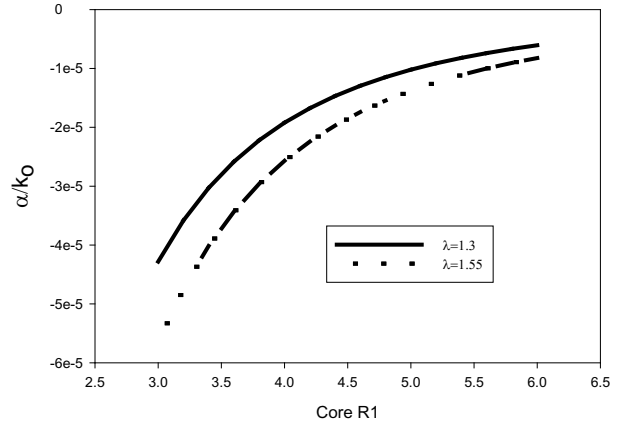

Fig. 8: A) Loss factor as a function of core radius at two different wavelengths

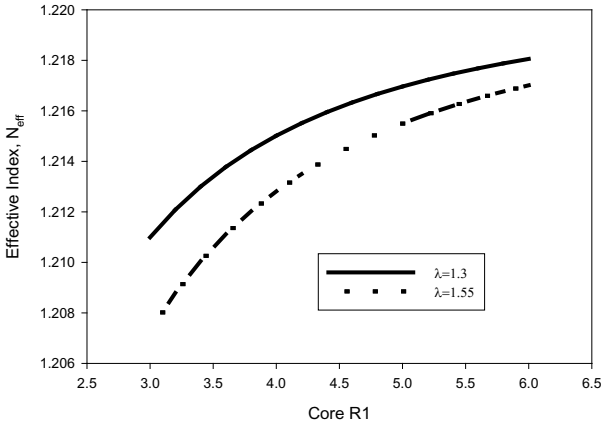

Fig. 8: B) Effective index as a function of core radius at two different wavelengths

Fig. 5 shows the profile of the field in both the x and y axial directions. As can be observed, a symmetrical profile is present in all directions. Such a profile ensures the integrity of the field. Figure 6 shows how the normalized field varies with the core radius of the fibre for two different wavelengths of interest. Fig. 7 on the other hand shows the dependence of the normalized Hx field profile on wavelength. It may be observed that the graph does not show a smooth dependence with sharp transitions. This may indicate that the field profiles are not uniformly confined at the various frequencies and should inform the design process. In Fig**.** 8 is shown the loss factor (Fig**.** 8A) and the effective index (Fig**.** 8B) for two different wavelengths as function of core radius. A parameter of interest is how the propagation constant and effective index will vary with wavelength. This is shown in Fig. 9. Fig. 9A shows the normalized propagation constant as a function of wavelength whilst Fig**.** 9B shows the effective index as a function of wavelength.

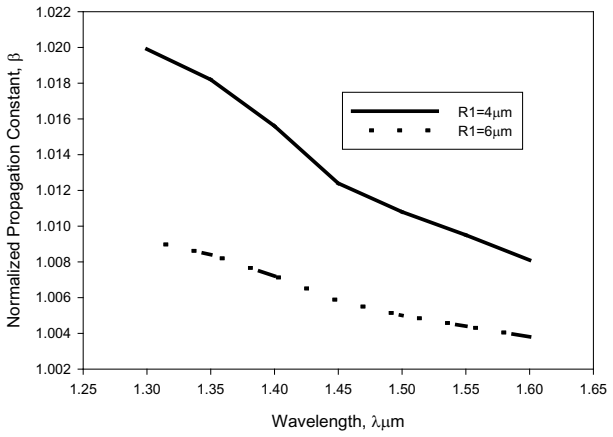

Fig. 9: A) Dependence of normalized propagation constant on wavelength for two different core sizes

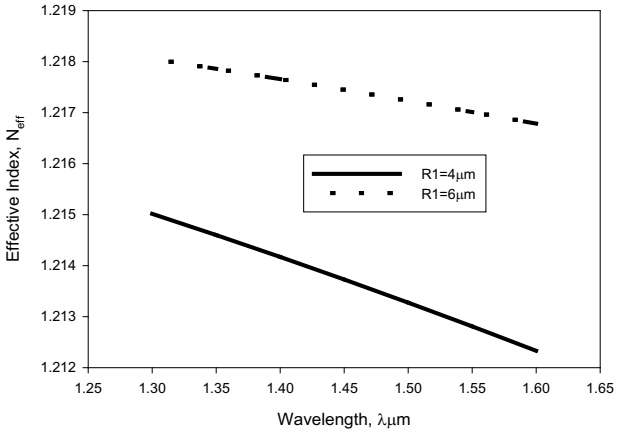

Fig. 9: B) Dependence of effective index on wavelength for two core radii

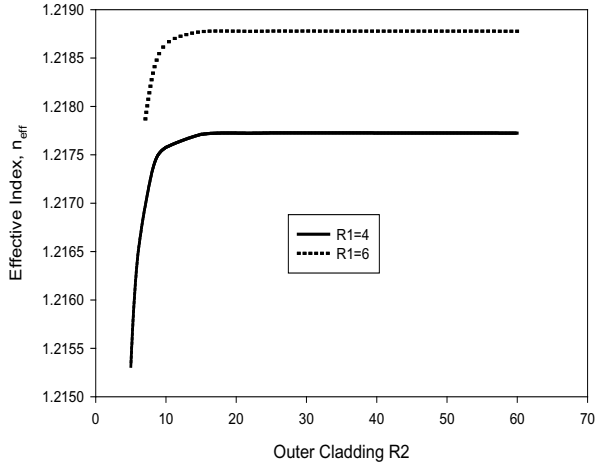

Fig. 10: A) Dependence of effective index on width of outer cladding for two different core sizes.

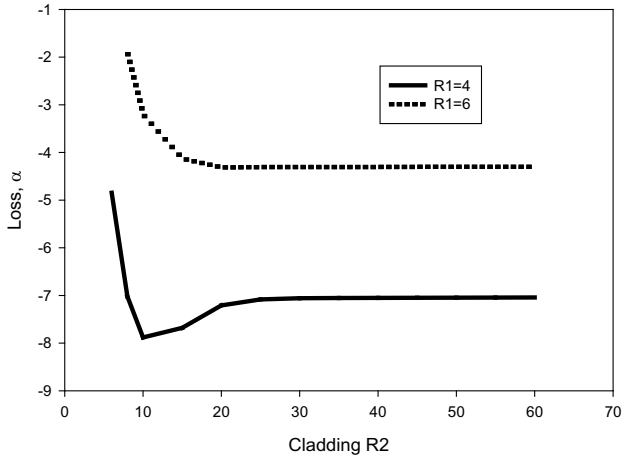

Fig. 10: B) Showing the loss factor for two different core sizes.

In each case, two different values of the core radius (R_1=4 μm and R_1=6 μm) are depicted. It can be observed that at a wavelength of λ=1.3 μm, for a core radius of 4 μm the normalized value of the propagation constant, β, is 1.020, and for a core radius of 6 μm, β=1.010, indicating a better confinement of the waves. On the other hand, the effective index of the smaller fibre core (R_1=4 μm) at the same wavelength of λ=1.3 μm is 1.215. For a core radius of R_1=6 μm, the value of the effective index is 1.218. This is entirely consistent with what is to be expected, since the higher the effective index, the better the waves will be propagated.

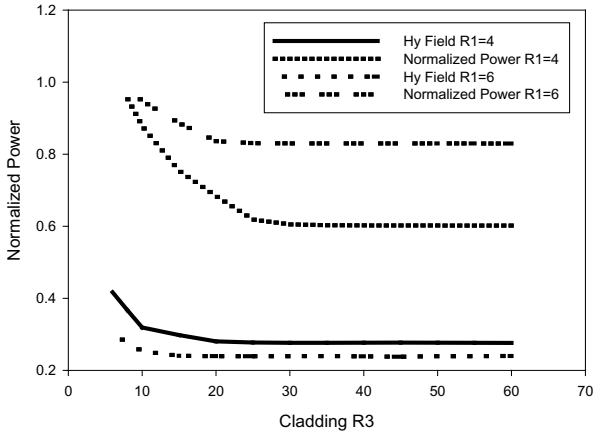

Fig. 11: A) Normalized values of power and field as function of outer cladding

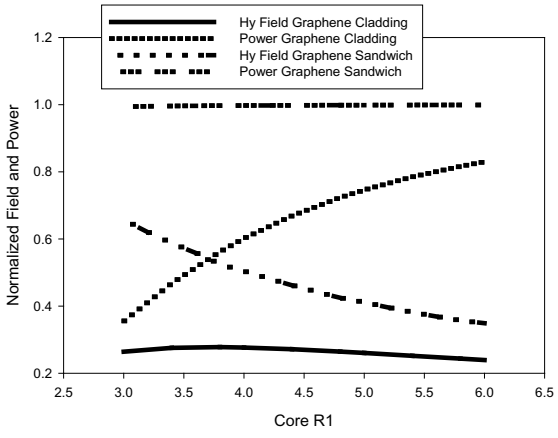

Fig. 11: B) Normalized values of power and field as a function of core diameter

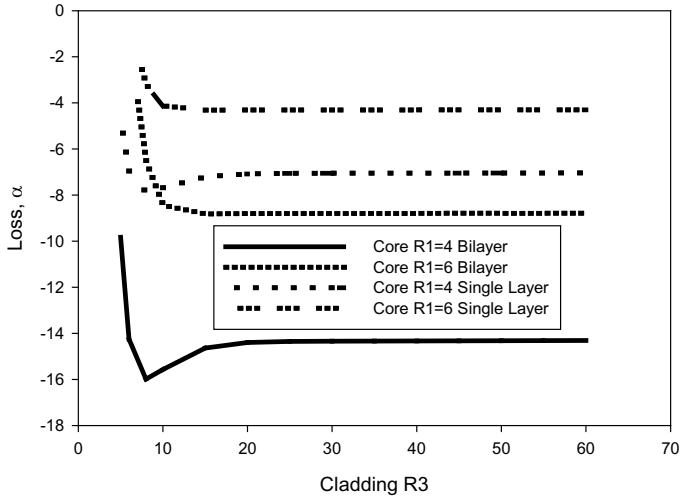

Fig. 12: Loss factor as a function of outer cladding for both single layer and double layer graphene

In the next simulations, an outer cladding is introduced to reflect the configuration of Fig. 1B. Figure 10 shows the results of the dependence of the effective index and the loss on the width of the outer cladding for two different core sizes. As will be expected, as the outer cladding is increased, the effective index also increases. However, beyond a certain point, in this case about 10 microns, any further increase in the cladding width does not impact on the results (Rahman and Davies, 1984). A sharp drop in loss factor at the point where the results become stable is worth noting. This drop may be attributed to transient instabilities.

Fig. 11A shows the normalized values for the H_y field and power for two different core sizes as the outer cladding is varied. Fig. 11B on the other hand shows the same parameters, but in this case, with the cladding width kept constant and the core size varied. In one case there is no outer cladding. With a constant value for the core region, we note that as cladding size is increased, the power within the core region decreases. However, if we keep the cladding constant and increase the core size, the power increases. This can be attributed to the fact that calculations for power are done within the core region, and the larger the core, the greater the power that is accounted for.

Results for Bilayer Configuration:

In some instances, it is found useful to use a number of layers of graphene (Hiura *et al.,* 2010). This may be due to the difficulty in obtaining a single sheet of the graphene. Usually, the maximum number of layers is assumed to be 3, as beyond this the material is no longer considered to be graphene (Miyazaki *et al.,* 2008; Pimenta *et al.,* 2007; Hiura *et al.,* 2010). In the next simulation, Fig. 12, it is shown how a two-layer graphene affects the simulation parameters. As in the previous simulations, two different core sizes are used, and the results or loss compared with that of a single layer configuration. It can be seen that the loss values for the bilayer devices are α=-15 for R_1= 6 and α=-9 for R_1=4. For the single layer α=-4 for R_1=6 and α=-8 for R_1=6. It may therefore be deduced that there is better confinement of the field in a double layer configuration.

Conclusion

Results for numerical analysis of a graphene cladded fibre have been presented. Two different structures were studied, a fibre core cladded with graphene but with no outer cladding and one in which there is an outer cladding. Single and double layer graphene structures have been investigated. Such a structure may find application as a nonlinear elements in pulse compression schemes. The results obtain show that it is possible to accurately model graphene cladded devices using the finite element method.

References

Bao, Q., Zhang, H., Wang, B., Ni, Z., Lim, C.H., Wang, Y., Loh, K.P. (2011). Broadband graphene polarizer, *Nature Photonics,* 5, 411-415.

Bao, Q., Zhang, H., Wang, Y., Ni, Z., Yan, Y., Shen, Z. X., Loh, K. P., Tang, D. Y. (2009). Atomic-layer graphene as a saturable absorber for ultrafast pulsed lasers. *Advanced. Functional. Materials*, 19, 3077-3083..

Bonaccorso F., Z. Sun, T. Hasan and A. C. Ferrari, (2010). Graphene Photonics and Optoelectronics, *Nature Photonics* 4, 611–622.

Themistos, C., Rahman, B.M.A., Markides, C, Uthman, M., Quadir, A. and Kejalakshmy, N. (2014). Characterization of graphene-based devices for THz systems, in Terahertz Physics, Devices, and Systems VIII: Advanced Applications in Industry and Defense, Mehdi F. Anwar; Thomas W. Crowe; Tariq Manzur, Editors, Proceedings of SPIE Vol. 9102 (SPIE, Bellingham, WA 2014), p. 91020F.

Miyazaki, H., Odaka, S., Sato, T., Tanaka, S., Goto, H., Kanda, A., Tsukagoshi, K., Ootuka, Y. and Aoyagi, Y. (2008). Inter-Layer Screening Length to Electric Field in Thin Graphite Film. *Appl. Phys. Express 1* (2008) 034007 -1-034007-3.

Hiura, H., Miyazaki, H. and Tsukagoshi, K. (2010). Determination of the Number of Graphene Layers: Discrete Distribution of the Secondary Electron Intensity Stemming from Individual Graphene Layers. *Applied Physics Express*, Volume 3, Number 9 , p.095101-1-095101-3

Huan Li, Yoska Anugrah, Steven J. Koester, and Mo Li, (2012). Optical absorption in graphene integrated on silicon waveguides, *Appl. Phys. Lett.* 101 (11) 111110-1-111110-5.

Inoue, T. and Namiki, S. (2008). Pulse compression techniques using highly nonlinear fibers, *Laser Photon. Rev*. 2, 83–99.

Katsriku, F.A. (2000). 'Finite element study of the second order (X^2) non-linear process of second harmonic generation in optical waveguides.' PhD Thesis, City University, London.

Keilmann, (2012). Trapping light in a carbon net, *Graphene Research*, Ludwig-Maximilians-Universitat Munchen. Available at https://www.en.uni-muenchen.de/news/newsarchiv/2012/2012_keilmann.html. Accessed 17th November 2017.

Kim, J.T. and Choi, S.Y. (2011). Graphene-based plasmonic waveguides for photonic integrated circuits, *Optics Express*, Nov. 21, 19(24), 24557-62.

Liu, M., Yin, X. and Zhang, X. (2012). Double-Layer Graphene Optical Modulator, *Nano Letters*, March 14, 12(3), 1482-5.

Liu, M., Yin, X., Ulin-Avila, E., Geng, B., Zentgraf, T., Ju, L., Wang, F. and Zhang, X. (2011). A graphene-based broadband optical modulator, *Nature*, 474, 64-67.

Novoselov, K.S., Jiang, Z., Zhang, Y., Morozov, S.V., Stormer, H.L., Zeitler, U., Geim, A.K. (2007). Room-Temperature Quantum Hall Effect in Graphene, Science, 315(5817), p. 1379.

Huang, P.L., Lin, S.C., Yeh, C.H., Kuo, H.H., Huang, S.H., Gong-Ru Lin, Cheng, W.H. (2012). Stable mode-locked fiber laser based on CVD fabricated graphene saturable absorber Optics Express 20 (3), 2460-2465.

Pimenta, M. A., Dresselhaus, G., Dresselhaus, M. S., Cancado, L. G., Jorio, A., Saito, R. (2007). Studying disorder in graphite-based systems by Raman spectroscopy. *Phys. Chem.* 9 (11), 1276 -1291.

Pumera, M. (2011), Graphene in Biosensing, *Materials Today*, 14(7-8), 308-315.

Rahman, B.M.A. and Davies, J.B. (1984). Penalty function improvement of waveguide solution by finite element. *IEEE Transactions on Microwave Theory Techniques MTT*-32 (8), 922-928.

Sensale-Rodriguez, B., Yan, R., Kelly, M. M., Fang, T., Tahy, K., Hwang, W. S., …Xing, H. G. (2012). Broadband graphene terahertz modulators enabled by intraband transitions, *Nature Communications*, 3 (780) 1-7.

Sun, Z., Hassan, T., Torrisi, F., Popa, D., Privitera, G., Wang, F., … Ferrari, A.C. (2010). Graphene mode-locked ultrafast laser, ACS Nano, 4, 803-813.

Sun, Z., Popa, D., Hasan, T., Torrisi, F., Wang, F., Kelleher, E.J.R, Ferrari, A.C. (2010). A Stable, Wideband Tunable, Near Transform-Limited, Graphene-Mode-Locked, Ultrafast Laser, Nano Research, 3(9): 653-660.

Thomas, M., Fengnian, X. and Phaedon, A. (2010). Graphene photodetectors for high-speed optical communications, *Nature Photonics*, 4, 297-301.

Zhang, H., Tang, D. Y., Zhao, L. M., Bao, Q. L., Loh, K. P. (2009). Large energy mode locking of an erbium-doped fiber laser with atomic layer graphene. *Opt. Express*, *17*, 17630–17635.

Zhu, S., Quarterman, A.H., Wonfor, A., Penty, R.V. and White, I.H. (2014) *Generation of 140 fs pulse train with widely tunable repetition rate through cascaded fibre compression techniques.* IET Optoelectronics, 8. 108-112